International Conference on Mathematics, Computational Methods & Reactor Physics (M&C 2009)
Saratoga Springs, New York, May 3-7, 2009, on CD-ROM, American Nuclear Society, LaGrange Park, IL (2009)

KERNEL DENSITY ESTIMATED MONTE CARLO GLOBAL FLUX TALLIES

Kaushik Banerjee and William R. Martin
Nuclear Engineering and Radiological Sciences, University of Michigan
Ann Arbor, MI 48109
bkaushik@umich.edu; wrm@umich.edu

ABSTRACT

The Kernel Density Estimator (KDE) is used to represent Monte Carlo (MC) tallies. Two new neutron flux estimators and their variances are developed, namely the KDE-collision and KDE-track-length. These new estimators are capable of estimating the flux at any point within a given domain without any bin structure. The strength of these two estimators is illustrated with numerical examples in 1D geometry. Convergence properties of the KDE estimators are discussed and the KDE estimators are compared with the Functional Expansion Tally (FET) and the conventional Histogram tally. The results show that the KDE tallies compare favorably with the FET and Histogram tallies with respect to accuracy and convergence rate.

Key Words: KDE, Monte Carlo Tallies, Convergence of Monte Carlo Tallies

1. INTRODUCTION

The Kernel Density Estimator (KDE), which is a nonparametric density estimator, can be used to represent Monte Carlo (MC) tallies with higher order shape information [1]. In nonparametric density estimation there is no a priori assumption about the functional form of the distribution associated with the random variable. In essence, the data are allowed to speak for themselves. In the conventional MC calculation histograms are used to represent tallies over bins which divide the phase space. Partitioning the phase space into bins can add significant overhead to a MC simulation. The KDE method is attractive because it can estimate MC tallies in any location within the required domain without any particular bin structure. Post-processing of the KDE tallies is sufficient to extract detailed tally information for an arbitrary grid. In this paper we will introduce the mathematical form of two new neutron flux estimators, viz. KDE-collision and KDE-track-length estimators, including their variances. Convergence properties of the KDE tally, the Functional Expansion Tally (FET) [2], and the histogram tally are also investigated. Convergence analyses of these estimators has been reported previously [3, 4, and 5] and a detailed analytical and numerical convergence comparison between the FET and histogram tallies was carried out by Griesheimer et al. [2]. As KDE estimated MC tallies are quite new to the nuclear science and engineering community, we are presenting here a very simplified analysis of the KDE convergence properties. This work is mainly based on the analysis done by Silverman [3]. The convergence properties of the FET and histogram tallies are also discussed from a different perspective than that in the paper by Griesheimer et al. [2]. The essence of this summary is the analytical and numerical comparison between the three estimators, namely KDE, FET, and histogram, which is not readily available in the existing literatures.

2. KERNEL DENSITY ESTIMATED MC GLOBAL FLUX TALLY

Consider *N* real observations $X_1,.....,X_N$ whose underlying density ($f(x)$) is to be estimated. The kernel density estimator with kernel *k* for univariate data is defined by

$$\hat{f}(x)=\frac{1}{Nh}\sum_{i=1}^{N}k\left(\frac{x-X_i}{h}\right), \tag{1}$$

where *h* ($h\to 0\, as\, N\to\infty$) is the bandwidth, also called the smoothing parameter. The bandwidth calculation and the form of the kernel function *k* will be discussed later in this paper. Generally the kernel *k* is a symmetric density function about zero and has the following properties:

$$\int k(t)dt=1,\ \int tk(t)dt=0,\ and\ \int t^2k(t)dt=k_2\neq 0. \tag{2}$$

From the definition of the KDE and the conventional collision flux tally we can easily derive the kernel density estimated collision flux tally and its variance:

$$\Phi(x)=\frac{1}{N}\sum_{i=1}^{N}\sum_{c=1}^{C_i}\frac{w_{i,c}}{\Sigma_t(X_{i,c})}\frac{1}{h}k\left(\frac{x-X_{i,c}}{h}\right), \tag{3}$$

$$\sigma^2_{\Phi(x)}=\frac{\frac{1}{N}\sum_{i=1}^{N}\left\{\sum_{c=1}^{C_i}\frac{w_{i,c}}{\Sigma_t(X_{i,c})}\frac{1}{h}k\left(\frac{x-X_{i,c}}{h}\right)\right\}^2-\left\{\frac{1}{N}\sum_{i=1}^{N}\sum_{c=1}^{C_i}\frac{w_{i,c}}{\Sigma_t(X_{i,c})}\frac{1}{h}k\left(\frac{x-X_{i,c}}{h}\right)\right\}^2}{N-1}, \tag{4}$$

where *c* is a sequential index of collision events for particle *i* at location $X_{i,c}$ and $w_{i,c}$ is the weight of particle *i* prior to collision *c*. The weights are important if variance reduction techniques are used. The quantity *N* is the total number of neutron histories. In a similar fashion, using the definition of the conventional track-length estimator the KDE track length tally and its variance are obtained:

$$\Phi(x)=\frac{1}{N}\sum_{i=1}^{N}\sum_{c=1}^{C_i}\frac{w_{i,c}d_{i,c}}{n}\sum_{j=1}^{n}\frac{1}{h}k\left(\frac{x-X_{i,c,j}}{h}\right), \tag{5}$$

$$\sigma^2_{\Phi(x)}=\frac{\frac{1}{N}\sum_{i=1}^{N}\left\{\sum_{c=1}^{C_i}\frac{w_{i,c}d_{i,c}}{n}\sum_{j=1}^{n}\frac{1}{h}k\left(\frac{x-X_{i,c,j}}{h}\right)\right\}^2-\left\{\Phi(x)\right\}^2}{N-1}, \tag{6}$$

where $d_{i,c}$ is the track length between events c and $c-1$. The KDE estimated track-length tally is implemented by dividing a single track into *n* uniform sub-tracks and by randomly selecting

points ($X_{i,c,j}$) from each sub-track. As noted previously [3], KDE has problems at boundaries due to the potential overlapping of an individual kernel and the boundary. To remedy this, we have used the boundary kernel method [6] as the boundary correction for the KDE tallies.

2.1. Numerical Examples of KDE Flux Tallies

An array of 6 1D fuel regions, each surrounded by water and with reflecting external boundaries to represent an infinite lattice, is used to estimate the scalar flux using KDE and FET. At the center of the array there is a strong neutron absorber. For a reference solution, a one energy group MCNP5 [7] kcode calculation is used with 500 cycles (200 inactive) and 200,000 histories per cycle. The scalar flux is estimated by employing the FMESH tally with 140 fine meshes in the x-direction. The KDE and FET estimations employed 30,000 histories per cycle for 200 cycles with the first 100 cycles discarded. Twelve Legendre expansion coefficients are used for the FET calculation.

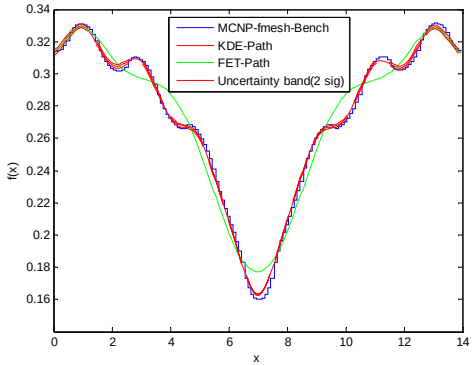

Figure 1. One group flux distribution inside a 1D array of fuel and water with strong neutron absorber in the center by track-length estimators.

In Fig. 1 the KDE-track-length estimator is calculated by using a single (global) bandwidth over the entire problem domain. In this case all the points extracted from the tracks during an active cycle need to be stored in order to calculate the bandwidth.

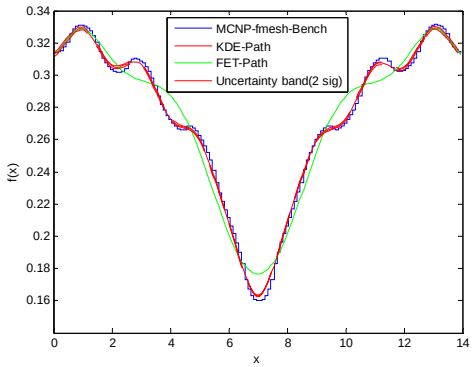

Figure 2. KDE-track-length scalar flux estimator without storing the points from the tracks in a neutron cycle.

At the end of each active cycle the bandwidth is calculated from the stored data and is then used for the subsequent KDE flux calculation for that cycle. The plotted flux is the average over the active cycles. That means at each cycle we need to store the data points, either collision points or points from tracks, in order to calculate the bandwidth at the end of the cycle. This storage requirement can be eliminated during a neutron cycle by using the bandwidth from the previous cycle. As the bandwidth depends mainly on the standard deviation of the data and number of data points, the bandwidth can be calculated in a cycle without storing the data points and that bandwidth can be used to score the KDE flux in the next cycle. The KDE-track-length tally without storing the points is illustrated for the same problem in Fig. 2. The KDE estimators can be slightly improved by using region based bandwidths instead of one global bandwidth. The KDE-collision and KDE-track-length estimators with material-region-based bandwidths are illustrated in Figs. 3 and 4. The reference solution for the collision tally is obtained with a benchmark calculation with 140 histogram bins in the x-direction, with 100,000 histories per cycle with 400 cycles and 200 discarded cycles. Note that for KDE estimation the internal shape of the flux is not dependent on placing bins within the material regions. The boundary correction for the KDE estimators is only used for the external boundaries and not for the internal material boundaries.

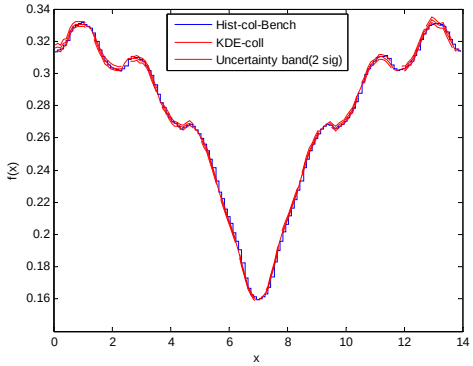

Figure 3. KDE-collision scalar flux estimator without storing the collision points in a neutron cycle and with region based bandwidths.

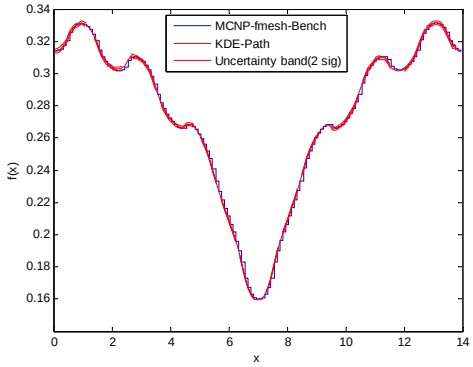

Figure 4. KDE-track-length scalar flux estimator without storing the points from the tracks in a neutron cycle and with region based bandwidths.

3. CONVERGENCE ANALYSIS

The Mean Integrated Square Error (*MISE*) is used as a measure of the discrepancy between the actual and the estimated density. The *MISE* is defined as follows

$$MISE(\hat{f}) = E\int\left\{\hat{f}(x) - f(x)\right\}^2 dx = \int\left\{E\hat{f}(x) - f(x)\right\}^2 dx + \int \text{var}\ \hat{f}(x)dx = bias\ +\ variance. \quad (7)$$

The actual density is given by $f(x)$, and the estimated density is denoted $\hat{f}(x)$. The term *E* is the expectation operator and the limit of the integration, if not explicitly given, is from negative infinity to positive infinity, which has been assumed for simplicity. All the analyses are also applicable to the boundary kernels used for correcting the boundary bias for KDE. These analyses are easily extended to multi-variate densities.

3.1 Convergence Analysis of the KDE Tally

For each x, $\hat{f}(x)$ in Eq. (1) can be considered as a random variable that depends on the observations $X_1, ..., X_N$. The bias and variance of the estimator are given by [3]

$$bias \approx \frac{1}{2}h^2 f''(x)k_2 + Higher\ Order\ Terms\ in\ h, \quad (8)$$

$$\text{var}\ \hat{f}(x) \approx \frac{1}{Nh} f(x)\int k(z)^2 dz + O\left(\frac{1}{N}\right). \quad (9)$$

The *MISE* can be approximated easily by combining Eqs. (7), (8) and (9) to find:

$$MISE\left(\hat{f}\right) \approx \frac{1}{4}h^4 k_2^2 \int f''(x)^2\, dx + \frac{1}{Nh}\int k(z)^2\, dz. \quad (10)$$

The basic assumption here is that the true density *f* is such that its second derivative f'' is continuous and square integrable. It is straightforward to derive the optimum bandwidth by minimizing the *MISE*:

$$\frac{\partial MISE}{\partial h} = h^3 k_2^2 \int f''(x)^2\, dx - \frac{1}{Nh^2}\int k(z)^2\, dz = 0$$

$$\Rightarrow h_{opt} = \frac{\left\{\int k(z)^2\, dz\right\}^{1/5}}{k_2^{2/5}\left\{\int f''(x)^2\, dx\right\}^{1/5}} N^{-1/5}. \quad (11)$$

A natural approach for calculating the bandwidth *h* is to use a standard family of distributions, like the Gaussian distribution, to obtain a value of the term $\int f''(x)^2\, dx$ in the Eq. (11). We can

derive an expression for the bandwidth *h* by also using a Gaussian function as the kernel function *k*:

$$h = 1.06\sigma N^{-1/5}. \tag{12}$$

The quantity σ^2 is the variance of the normal distribution and can be estimated by the usual standard deviation of the data or by some more robust estimators. The bandwidth in Eq. (12) is used for all our simulations. For the region based bandwidths we calculated the σ and *N* (number of collisions or the number of points extracted from the tracks generated in a particular material region) for each region.

Inserting the optimum bandwidth into the *MISE* equation (Eq. (10)) we can arrive at the final approximate expression for *MISE*:

$$\begin{aligned} MISE\left(\hat{f}\right)_{KDE} &= \frac{5}{4}C(k)\left\{\int f''(x)^2\,dx\right\}^{1/5} N^{-4/5} \\ &= O\left(N^{-4/5}\right), \quad \left[in\ leading\ order\ term\right] \end{aligned} \tag{13}$$

where

$$C(k) = k_2^{2/5}\left\{\int k(z)^2\,dz\right\}^{4/5}. \tag{14}$$

C(k) can be minimized by using the Epanechnikov kernel [3] which is given by

$$k(x) = \begin{cases} \dfrac{3}{4\sqrt{5}}\left(1-\dfrac{x^2}{5}\right), & |x| \le \sqrt{5} \\ 0, & otherwise \end{cases}. \tag{15}$$

The kernel function *k* in Eq. (15) is used for all our simulations.

3.2 Convergence Analysis of the FET tally

This analysis is a variation on the analysis performed by Griesheimer et al. [2]. If $\left[\psi_n\right]_0^\alpha$ is a complete orthogonal set with respect to some weighting function $\rho(x)$ in $L_\rho^2(\Gamma)$, which is the space defined by all square integrable functions over some bounded domain Γ, then any $f(x) \in L_\rho^2(\Gamma)$ can be written as

$$f(x) = \sum_{n=0}^{\infty} \bar{a}_n k_n \psi_n(x), \tag{16}$$

where $\bar{a}_n$ is the nth expansion coefficient defined by (using the orthogonality properties of the basis functions)

$$\bar{a}_n = \int \psi_n(x)\rho(x)f(x)dx, \tag{17}$$

and k_n is the normalization constant for the nth basis function [2]. As it is not possible to calculate an infinite number of terms, the estimator ($\hat{f}(x)$) of the true function f is always truncated to some finite number *M*:

$$\hat{f}(x) = \sum_{n=0}^{M} \hat{a}_n k_n \psi_n(x), \tag{18}$$

where

$$\hat{a}_n = \frac{1}{N}\sum_{i=1}^{N} \psi_n(X_i)\rho(X_i). \tag{19}$$

It is easy to derive the first term of the *MISE* expression in Eq.(7):

$$\begin{aligned}\int \left\{E\hat{f}(x) - f(x)\right\}^2 \rho(x)dx &= \int \left(\sum_{n=M+1}^{\infty} k_n \bar{a}_n \psi_n(x)\right)^2 \rho(x)dx \\ &= \int \left(\sum_{n=M+1}^{\infty}\sum_{m=M+1}^{\infty} k_n k_m \bar{a}_n \bar{a}_m \psi_n(x)\psi_m(x)\right)\rho(x)dx \\ &= \sum_{n=M+1}^{\infty} \bar{a}_n^2 k_n.\end{aligned} \tag{20}$$

Equation (20) is obtained by using the orthogonality property of the basis functions. The true expansion coefficients converge at a rate determined by κ [8, 9]

$$|\bar{a}_n| = O\left(\frac{1}{n^{\kappa}}\right). \tag{21}$$

The value of κ, which is called the algebraic index of convergence, is generally equal to the number of derivatives of the true density function *f* that are square integrable [8, 9]. Using Eqs.(20) and (21) the integral of the square bias term can be written as

$$\begin{aligned}\int \left\{E\hat{f}(x) - f(x)\right\}^2 \rho(x)dx &\approx \sum_{n=M+1}^{\infty} O\left(\frac{1}{n^{2\kappa}}\right)\frac{2n+1}{2}, \left[\textit{ for Legendre polynomials}\right] \\ &\approx O\left(\frac{1}{M^{2\kappa-2}}\right).\end{aligned} \tag{22}$$

The last line in Eq. (22) is obtained by using an infinite series summation [10]. The second term of the MISE in Eq. (7) can be written as [2]

$$\int \text{var}\ \hat{f}(x)\rho(x)dx \approx O\left(\frac{M}{N}\right). \tag{23}$$

Finally, the results from Eqs. (22) and (23) can then be used to write the *MISE* of FET as

$$MISE\left(\hat{f}\right)_{FET} = O\left(\frac{1}{M^{2\kappa-2}}\right) + O\left(\frac{M}{N}\right). \tag{24}$$

The *MISE* of FET can be minimized over *M* by simple calculus

$$M_{opt} = O\left(N^{1/2\kappa-1}\right). \tag{25}$$

Substituting the optimum *M* into Eq. (24) we obtain

$$MISE\left(\hat{f}\right)_{FET} = O\left(N^{-\frac{2\kappa-2}{2k-1}}\right). \tag{26}$$

3.3 Convergence Analysis of the Histogram Tally

Let us assume N_b is the number of observations in bin *b* and *M* is the total number of bins. Also, *N* is the total number of observations and Δx (L/M, where *L* is the length of the domain) is the width of each bin. The width of the bins is taken constant for this analysis. The bias of the histogram estimator for bin *b* can be written as

$$\begin{aligned} bias_{M,b} &= E\hat{f}_{M,b}^{hist} - f(x) \\ &= \frac{1}{\Delta x}\int_{x_{b-1}}^{x_b} f(x)dx - f(x) \\ &\approx \frac{1}{\Delta x}\Delta x f\left(x_{b-1/2}\right) - \left\{ f\left(x_{b-1/2}\right) + \left(x - x_{b-1/2}\right) f'\left(x_{b-1/2}\right) + \frac{\left(x - x_{b-1/2}\right)^2}{2} f''\left(x_{b-1/2}\right) + \ldots \right\} \\ &\approx O\left(\Delta x\right). \end{aligned} \tag{27}$$

It is now simple to obtain an expression for the first term of the MISE in Eq. (7) for histogram

$$\int bias^2\left(x\right)dx \approx \sum_{b=1}^{M} O\left(\Delta x^2\right)\Delta x \approx \sum_{b=1}^{M} O\left(\frac{L^3}{M^3}\right) \approx \sum_{b=1}^{M} O\left(\frac{1}{M^3}\right) = O\left(\frac{1}{M^2}\right). \tag{28}$$

The histogram estimator can be expressed as

$$\hat{f}^{hist}(x) = \frac{1}{N\Delta x}\sum_{i=1}^{N} I\{X_i \in b\}, \quad x \in [x_{b-1}, x_b]. \tag{29}$$

The random variable $I\{X_i \in b\}$ is associated with Bernoulli's distribution, whose variance is given by $p(1-p)$, where p can be written as

$$p = \int_{x_{b-1}}^{x_b} f(x)dx. \tag{30}$$

The variance of the histogram estimator can be calculated as

$$\begin{aligned} \text{var}\ \hat{f}^{hist}(x) &= \frac{1}{N^2\Delta x^2}\sum_{i=1}^{N} \text{var}\, I \\ &= \frac{1}{N^2\Delta x^2} N\left\{\int_{x_{b-1}}^{x_b} f(x)dx\left(1-\int_{x_{b-1}}^{x_b} f(x)dx\right)\right\} \\ &\approx \frac{1}{N\Delta x} f(x_{b-1/2}). \end{aligned} \tag{31}$$

It is now straightforward to calculate the second term of MISE in Eq. (7) for a histogram:

$$\int \text{var}\ \hat{f}^{hist}(x)dx \approx \int \frac{1}{N\Delta x} f(x_{b-1/2})dx \approx O\left(\frac{M}{N}\right). \tag{32}$$

Equations(7),(28), and (32) yield

$$MISE\left(\hat{f}\right)_{hist} = O\left(\frac{1}{M^2}\right) + O\left(\frac{M}{N}\right). \tag{33}$$

By simple calculus we can easily derive the optimum number of bins, yielding

$$M_{opt} \approx O\left(N^{1/3}\right). \tag{34}$$

Substituting the value of M from Eq. (34) into Eq. (33) we find

$$MISE\left(\hat{f}\right)_{hist} = O\left(N^{-\frac{2}{3}}\right). \tag{35}$$

4. COMPARISON AMONG KDE, FET, AND HISTOGRAM RESULTS

The KDE, FET, and histogram approximations of the true distribution converge at different rates dependent on the problem parameters. However, for most of the cases the KDE tally outperforms the FET tally, which in turn outperforms the histogram tally. If we consider $\kappa = 2$, that means the underlying true density function *f* has two integrable derivatives, then from Eqs. (13) and (26) it is easy to conclude that the $MISE\left(\hat{f}\right)_{KDE}$ has a faster convergence rate than $MISE\left(\hat{f}\right)_{FET}$. Although the KDE *MISE* calculation assumed that the second derivative f'' of the true density is continuous and square integrable, it is evident from the Figs. 1-4 that global KDE can estimate the material discontinuity within the domain much more effectively than the global FET. For FET estimation the material discontinuity can only be taken care by piecewise FET approximation. A significant feature of the KDE tally, which is shared by the FET tally, is that internal structure within the bin can be obtained without resorting to bin refinement. However, the FET tally requires a knowledge of the bin boundaries since the expansion functions are defined over the bin while the KDE tally is independent of the bin boundaries because the kernels are defined only at the interaction point. Because of this, we believe that the KDE tally will allow the pathlength estimator to be used when Woodcock tracking [11] is employed. Finally, the KDE performance can be improved further by using higher order kernels. In this analysis we assume k_2 (second moment of the kernel *k*) in Eq. (2) is not equal to zero. However if we relax this restriction, it is possible to construct *k* with $k_2 = 0$, which will further reduce the bias of the estimator.

5. NUMERICAL VERIFICATION OF CONVERGENCE

We now present a series of numerical experiments to verify the convergence analyses of the three tallies discussed above. The same trial distribution $f(x)$ is used in each numerical experiment,

$$f(x) = \frac{1}{1.51985}\begin{cases} \cos(x)e^{2x+1}, & x \in [-1,-1/2], \\ \cos(x), & x \in [-1/2,1/2], \\ \cos(x)e^{-x/2+1/4}, & x \in [1/2,1]. \end{cases} \tag{36}$$

In the first set of experiments the integrated bias square and the integrated variance of each of the estimator are calculated for the trial distribution $f(x)$. The integrated square bias and the integrated variance for KDE are plotted separately in Fig. 5 vs. bandwidth *h* where 10,000 histories are used. The entire domain *[-1, 1]* is divided into *B (50)* bins and the density is estimated at the mid point of each bin. The calculation is repeated *n (50)* times to estimate the expectation. The sum of the integrated square bias and the integrated variance, which is the *MISE*, is also plotted in the same plot. The *MISE* of the KDE has a minimum point which corresponds to the optimum bandwidth. The integrated bias for all three estimators is calculated as follows

$$\int \left\{ E\hat{f}\left(x\right) - f\left(x\right) \right\}^2 dx \approx \sum_{i=1}^{B} \left\{ E\hat{f}\left(x_i\right) - f\left(x_i\right) \right\}^2 \Delta x, \tag{37}$$

where Δx is the bin width. The variance is calculated as the sample variance.

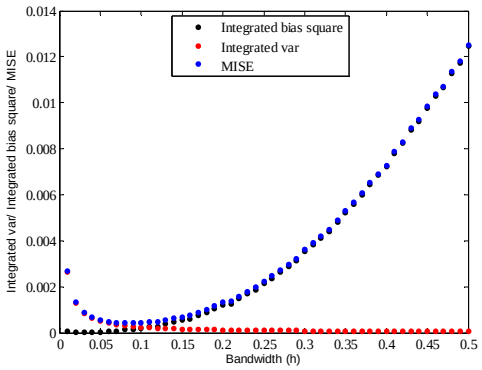

Figure 5. Plot of integrated variance, integrated bias square and MISE vs. bandwidth for KDE.

The same experiment is carried out for FET and histogram and results are illustrated in Figs. 6 and 7. The minimum point of the *MISE* in Fig. 6 corresponds to the optimum number of expansion coefficients for FET. The optimum number of bins for the histogram is predicated by the minimum *MISE* in Fig. 7.

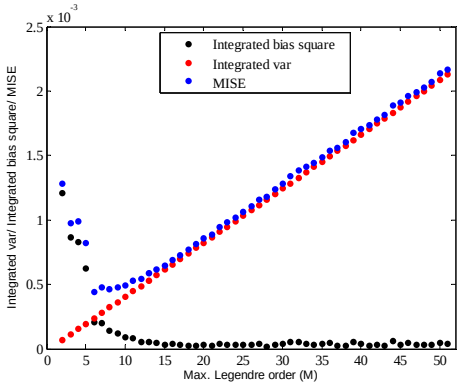

Figure 6. Plot of integrated variance, integrated bias square and MISE vs. number of expansion coefficients for FET.

Finally, the MISE is plotted versus the number of histories in Fig. 8. The MISE is calculated as follows

$$MISE = \frac{\sum_{j=1}^{n} \sum_{b=1}^{B} \left\{ \hat{f}_{b,j} - f_b \right\}^2 \Delta x}{n} \tag{38}$$

The optimum values of the bandwidth (KDE), the number of terms (FET), and the number of bins (histogram), which vary with the number of histories, are used in this plot (Fig. 8).

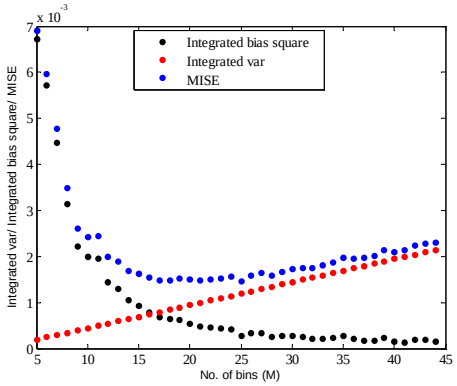

Figure 7. Plot of integrated variance, integrated bias square and MISE vs. number of bins for histogram.

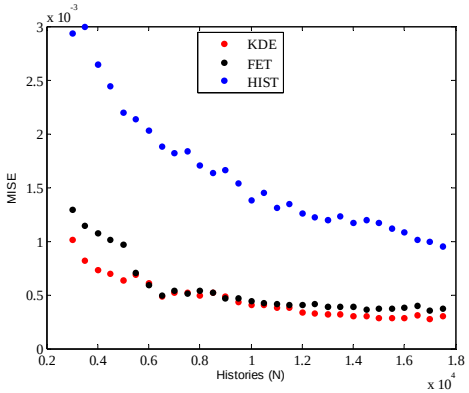

Figure 8. Plot of *MISE* vs. number of histories *N* for KDE, FET, and histogram tallies.

6. DISCUSSION

The advantages of the KDE tallies over the FET and histogram tallies have been shown. The primary disadvantage of KDE for a criticality calculation is the requirement of storing all the points (collision points or *n* points from each track) during a cycle for calculating the bandwidth (*h*) at the end of the cycle. That disadvantage has been successfully overcome by using the bandwidth from the previous batch for the criticality calculations. The bandwidth can be calculated online since it mainly depends on the standard deviation. So the remedy is to start calculating the bandwidth just before the active cycles begin as all the tallies are averaged only over the active cycles. A major advantage of the KDE tally is the elimination of internal bin structure to resolve the shape of the tally within a given region. Also, we conjecture that the KDE path-length tally can be used with Woodcock tracking. We will report on these topics in a future work.

REFERENCES

1. K. Banerjee and W. R. Martin, "Monte Carlo Global Scalar Flux Estimation with Kernel Density Estimator," *Trans. Am. Nucl. Soc.*, Reno, NV, 9-13th November, Vol. 99, pp. 346-347 (2008).
2. D. P. Griesheimer, W. R. Martin, and J. P. Holloway, "Convergence Properties of Monte Carlo Functional Expansion Tallies," *Journal of Computational Physics*, **211**, pp. 129-153 (2006).
3. B. W. Silverman, *Density Estimation for Statistics and Data Analysis*, Chapman and Hall, London (1986).
4. P. Hall, "On the Rate of Convergence of Orthogonal Series Density Estimators," *J. R. Statist. Soc. Series B (Methodology)*, **48**, pp. 115-122 (1986).
5. P. J. Diggle and P. Hall, "The Selection of Terms in an Orthogonal Series Density Estimator," *Journal of the American Statistical Association*, **81**, pp. 230-233 (1986).
6. M. C. Jones, "Simple Boundary Correction for Kernel Density Estimation," *Statistics and Computing*, **3**, pp. 135-146 (1993).
7. Monte Carlo Team, "MCNP – A General Monte Carlo N-Particle Transport Code, Version 5," *LA-UR-03-1987*, Los Alamos National Laboratory (2003).
8. J. P. Boyd, *Chebyshev & Fourier Spectral Methods*, Springer-Verlag, New York (1989).
9. D. P. Griesheimer, *Functional Expansion Tallies for Monte Carlo Simulations*, Ph.D. Thesis, Nuclear Engineering and Radiological Sciences, University of Michigan (2005).
10. C. M. Bender and S. A. Orszag, *Advanced Mathematical Methods for Scientists and Engineers*, McGraw-Hill, New York (1978).
11. E.R. Woodcock, T. Murphy, P.J. Hemmings, T.C. Longworth, "Techniques Used in the GEM Code for Monte Carlo Neutronics Calculations in Reactors and Other Systems of Complex Geometry," *Proc. Conf. Applications of Computing Methods to Reactor Problems*, ANL-7050, pp. 557, Argonne National Laboratory (1965).